Journal of Biomedical Optics

SPIEDigitalLibrary.org/jbo

Temporal and spatial temperature distribution in the glabrous skin of rats induced by short-pulse CO_2 laser

Pen-Li Lu
Shu-Shen Hsu
Meng-Li Tsai
Fu-Shan Jaw
An-Bang Wang
Chen-Tung Yen

SPIE

Temporal and spatial temperature distribution in the glabrous skin of rats induced by short-pulse CO_2 laser

Pen-Li Lu,[a] Shu-Shen Hsu,[b] Meng-Li Tsai,[c] Fu-Shan Jaw,[a] An-Bang Wang,[b] and Chen-Tung Yen[d]
[a]National Taiwan University, Institute of Biomedical Engineering, No. 1, Sec. 4, Roosevelt Road, Taipei 10617, Taiwan
[b]National Taiwan University, Institute of Applied Mechanics, No. 1, Sec. 4, Roosevelt Road, Taipei 10617, Taiwan
[c]National Ilan University, Department of Biomechatronic Engineering, No. 1, Sec. 1, Shen-Lung Road, I-Lan, 260, Taiwan
[d]National Taiwan University, Institute of Zoology and Department of Life Science, No. 1, Sec. 4, Roosevelt Road, Taipei 10617, Taiwan

Abstract. Pain is a natural alarm that aids the body in avoiding potential danger and can also present as an important indicator in clinics. Infrared laser-evoked potentials can be used as an objective index to evaluate nociception. In animal studies, a short-pulse laser is crucial because it completes the stimulation before escape behavior. The objective of the present study was to obtain the temporal and spatial temperature distributions in the skin caused by the irradiation of a short-pulse laser. A fast speed infrared camera was used to measure the surface temperature caused by a CO_2 laser of different durations (25 and 35 ms) and power. The measured results were subsequently implemented with a three-layer finite element model to predict the subsurface temperature. We found that stratum corneum was crucial in the modeling of fast temperature response, and escape behaviors correlated with predictions of temperature at subsurface. Results indicated that the onset latency and duration of activated nociceptors must be carefully considered when interpreting physiological responses evoked by infrared irradiation. [DOI: 10.1117/1.JBO.17.11.117002]

Keywords: infrared laser; heat pain stimulator; infrared camera; temperature distribution; finite element modeling; nociceptors.

Paper 12175 received Mar. 14, 2012; revised manuscript received Sep. 27, 2012; accepted for publication Oct. 2, 2012; published online Nov. 1, 2012.

1 Introduction

Pain is nature's alarm to the body to avoid potential danger. Congenital pain deficiency usually leads to limb and oral injuries or early death. In contrast, hypersensitivity to pain impairs the quality of life.[1,2] Pain is also a very useful indicator in clinical diagnosis. However, pain as a subjective experience is affected by age, gender, language, attention, former experience and many other factors. A precise, repeatable noxious stimulus is necessary to obtain an objective measure of pain sensation and pain responses.

Infrared laser is energy-controlled, highly reproducible heat pain stimulation.[3] Infrared laser irradiation evokes EEG potential changes in healthy humans.[4,5] These laser heat evoked potentials are objective indices of central processing of nociceptive information in the brain.[6,7] In addition, radiant heat stimulation is essential for wakeful, freely moving behavioral animal studies.[8–10] Short-pulse lasers of tens of milliseconds offer several advantages over a long-pulse laser, including completing noxious stimuli before escape behaviors,[8–10] reducing tissue damage, and increasing synchronization of neuronal activities.

Temperature distribution of infrared lasers affects the moment, period, and number of activated nociceptors. These further affect the conduction velocity, responsive period, and responsive magnitude of laser-evoked responses. A two-dimensional (2-D) axial model, instead of a one-dimensional (1-D), can provide sufficient information to simulate the activation of nociceptors. However, 2-D axial temperature distribution of short-pulse lasers remains unavailable. Current knowledge is based on a longer pulse duration (hundreds of milliseconds) in human data.[11,12] Currently, the precise distributions of short-pulse lasers are highly dependent on 1-D mathematic modeling with experimental validation[13] or rely on 1-D[14] or three-dimensional (3-D)[15] mathematic modeling without experimental validation.

Nociceptors are free nerve endings that can be activated by noxious stimuli. In rats, two major types of cutaneous nociceptors are distributed within epidermis, except stratum corneum.[16] One type is transmitted by myelinated Aδ fiber, called A-mechano-heat nociceptors (AMHs), and the other type is transmitted by unmyelinated C fiber, the C- mechano-heat nociceptors (CMHs). The thresholds of nociceptors vary in different studies. The thresholds of AMHs are above 47°C[17] and 43.8 ± 0.4°C[18] whereas the threshold of CMHs are 37–47°C, 50–52°C[17] and 55.4 ± 0.7°C.[18] This study assumed that 43°C at viable epidermis (40 to 90 μm[19,20] in depth) would activate a number of CMHs and AMHs. We calculated the onset latency, supra-threshold period, and maximal radius of 43°C at epidermis of 40 μm in depth.

The CO_2 laser was the first short-pulse infrared laser used for the study of pain.[3] Since then, the CO_2 laser has been widely used in human and animal pain studies.[8–10,21–23] We investigated six intensities of short-pulse (25 and 35 ms) CO_2 laser, which ranged from innocuous to noxious indicated by paw lifting. We applied laser pulses on the hind paw of the rat under anesthesia, and detected surface temperature distribution by a fast speed

Address all correspondence to: Chen-Tung Yen, National Taiwan University, Institute of Zoology and Department of Life Science, 1 Roosevelt Road, Sec. 4, Taipei 10617, Taiwan. Tel: +886-2-33662451; Fax: +886-2-23625048; E-mail: ctyen@ntu.edu.t

0091-3286/2012/$25.00 © 2012 SPIE

infrared camera. We simulated the surface temperature by a three-layer finite element model in 2-D and predicted subsurface temperature profiles. The results are beneficial to interpret the physiological responses induced by a CO_2 laser, as well as for assessing the thermal effects on tissue.

2 Materials and Methods

2.1 *Measurement of Surface Temperature*

An infrared camera was used (TVS-8500, NEC Avio Infrared Technologies, Tokyo, Japan), with a sampling rate of 120 frames per second. The camera, fixed on a tripod that continuously monitored the skin, had a spatial resolution of seven to 10 pixels per cm. A 2×2-cm copper plate was placed beneath the stimulation site to calibrate the spatial resolution. The camera received a transistor-transistor logic (TTL) signal to start frame capturing. A total of 600 frames were captured in every trial. The emission rate of the rat's paw was measured in a preliminary study ($n = 1$). The rat was anesthetized by sodium pentobarbital (65 mg/kg). A K-type thermal couple was placed tightly on the skin surface of the paw, which was then heated by a hairdryer from room temperature to 90°C. The skin temperature was measured by the thermal couple and the infrared camera, the purpose being that this procedure would cover the full range of the surface temperature change in our calibration of the infrared camera. The emission rate equaled 0.9, which was the linear correlation coefficient of temperatures measured by the infrared camera and the thermal couple.

2.2 *CO_2 Laser Machine*

The CO_2 laser (Blue Sky Tech., Taipei, Taiwan) operated at TEM_{00} mode and generated an infrared radiation beam (wavelength = 10,600 nm). Beam diameter was 3.5 mm, and the beam divergence was 4 mR, with a standard deviation of Gaussian fit of the laser profile (σ) being 0.875 mm. The target area of the laser beam was co-localized with a visible red light and its power and duration were adjustable, ranging from zero to 10 W and 99 ms, respectively. Five laser powers (1, 3, 5, 7, and 9 W) combined with 25-ms pulse duration were used, along with a 5 W-35 ms laser pulse. The CO_2 laser can receive a TTL signal to emit one pulse at 85 ms later (innate delay). The CO_2 laser was placed 9 cm above the rat's paw.

2.3 *Experimental Animals*

Three male Wistar rats (330, 550, and 610 gw) were anesthetized by sodium pentobarbital (65 mg/kg, i.p.), and their body temperatures were maintained at 37°C by a homeothermic blanket. The rat was laid on the table and the hind paw was fixed with tape. Supplemental anesthetic doses (20 mg/kg, i.p.) were administered if the rat exhibited signs of light and quick breathing and pinch reflex.

2.4 *Experimental Protocols*

One TTL signal was sent to the infrared camera and the CO_2 laser to trigger frame-capturing and single-pulse emission. We reconstructed the surface temperature by recording the first 11 consequent frames (8.3 ms interval) from temperature rising, subsequent nine of every five frames (41.5 ms interval), and the last frame (Fig. 1). The order of stimulation was 1 W-, 3 W-, 5 W-, and 7 W-25 ms, 5 W-35 ms, and 9 W-25 ms, with the interval between each laser pulse set at least 3 min to maintain the baseline temperate. The stimulation sites were slightly shifted during the experiment to prevent skin damage; the animals recovered from anesthesia after receiving 9 W-25 ms stimulation.

2.5 *Estimation of SubSurface Temperature by Finite Element Model*

We first used a two-layer fininte element model (FEM-2, Fig. 2), which was also used in a human study,[11] to represent the skin of the rat's paw. However, the simulation results were not satisfactory (see Sec. 3). Instead, we used a three-layer model (FEM-3, Fig. 2), which contains stratum corneum. The thickness of stratum corneum was 40 μm, and the remaining epidermis was 50 μm.[20] The dermis was 800 μm thick.[19] The thermal conductivity of stratum corneum and the viable epidermis was 0.1 $W/(m \times K)$ (Refs. 24 and 25) (K is the absolute temperature). The other parameters were set according to Frahm et al.[11] The temperature distribution was based on Pennes's bioheat

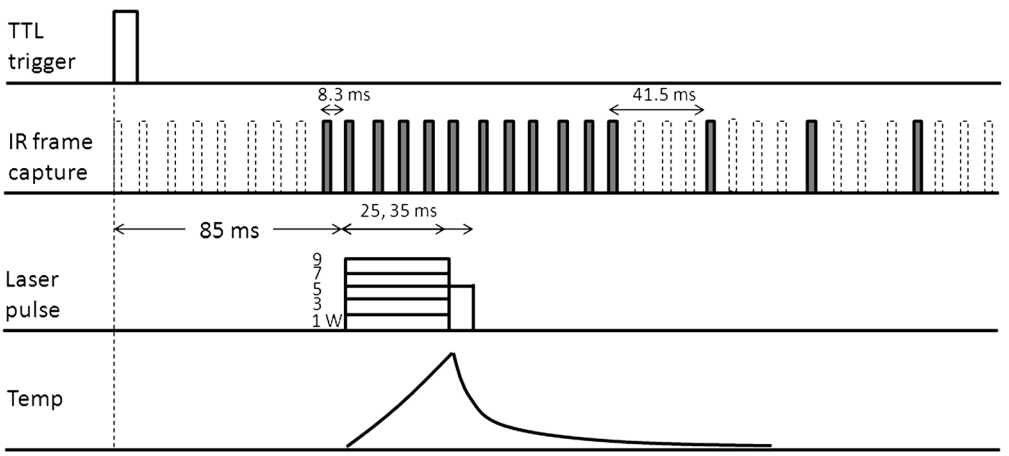

Fig. 1 Experimental protocols. TTL trigger immediately started frame capture of infrared camera (IR frame capture). TTL trigger also started a pulse of CO_2 laser 85 ms later (innate latency of CO_2 laser). The 11 consequent frames (8.3 ms interval) from temperature (Temp) rising, subsequent nine of every five frames (41.5 ms interval), and the last frame were recorded (filled blocks of IR frame capture).

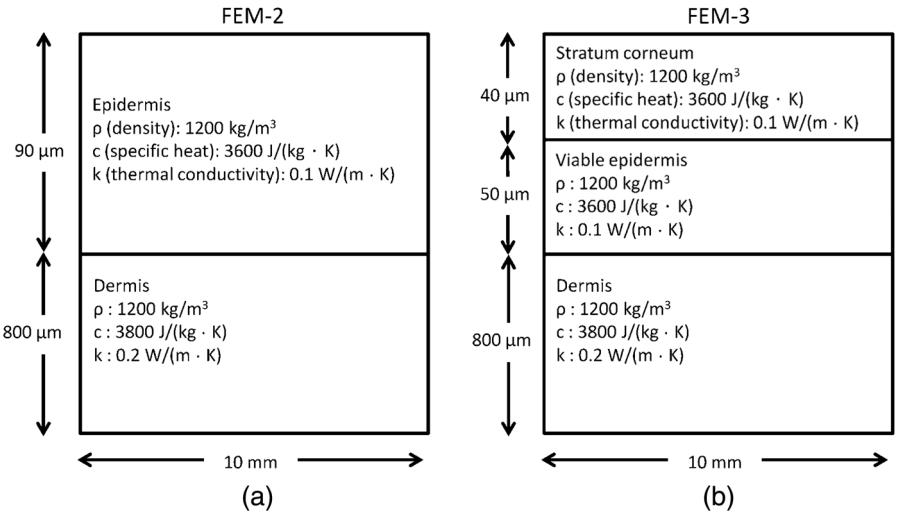

Fig. 2 Skin model of rat's paw. (a) Two-layer finite element model (FEM-2). (b) Three-layer finite element model (FEM-3).

equation [Eq. (1)].[26] The heat source (Q, W/m^2) was assumed as exclusively contributed by the laser, which is described by Eq. (2). The equation was solved by FEM in MatLab (pdetool, MathWorks, Natick, MA). We chose 3313 triangular elements to solve the equation. The lowest boundary of dermis was assumed as a constant temperature (Dirichlet condition, $\Delta T = 0$). The other boundary conditions were assumed to be thermal-isolated (Neumann condition, heat flux $= 0$). The heat-transfer coefficient (q) of every boundary was 3.5 W/m^{2}K.[27]

$$\rho c \frac{\partial T(r,t)}{\partial t} - \nabla[k \nabla T(r,t)] = Q(r,t), \tag{1}$$

$$Q(r,t) - P_m \mu_a e^{(-\mu_a Z)} \frac{1}{\sigma\sqrt{2\pi}} e^{\left(\frac{-r^2}{2\sigma^2}\right)}, \tag{2}$$

where ρ is tissue density, c is specific heat of tissue, T is tissue temperature, t is time, k is thermal conductivity, P_{in} is laser power (W), μ_a is the absorption coefficient of tissue assumed to contain 35% or 40% water (30,000 or 35,000 $1/m$), z is the depth from skin surface, σ is the standard deviation of Gaussian fit of the laser profile (0.875 mm), and r is the distance from the axis of the laser beam.

2.6 *Paw-Lifting Ratio Measurement*

The paw-lifting ratios of an additional 15 rats were measured when receiving laser heat stimulation. Rats were placed in a transparent box (size: $20 \times 26 \times 35$ cm) with a grid floor. Rats were habituated in the same environment half hour a day for 3 days before the measurement. The laser beam passed through the grid to stimulate the paw. Rats received laser stimulation only under a resting state, which was indicated by open eyes, standing still, regular breathing, and no whisker vibration. Ten shots of the laser were applied on the same paw, but shifted slightly. The inter-stimulus-interval was at least 20 s. Paw lifting ratio was the number of paw lifting among 10 stimuli, and presented in percentage.

2.7 *Data Analysis*

The onset latency, supra-threshold duration, and range of activated nociceptors were calculated from FEM-3 data. The onset latency was defined as the first instant that tissue at a depth of 40 μm reached 43°C. The supra-threshold duration was defined as the period that tissue at a depth of 40 μm reached 43°C. The maximal heating radius was defined as the maximal radius at a depth of 40 μm where temperature reached 43°C. The measured peak temperature of 5 W-25 ms and 7 W-25 ms were tested by Student's t test. The correlation between measured and predicted temperature on skin surface was conducted by Pearson product-moment correlation.[11] The intensities at which paw-lifting ratios exceeded baseline significantly as induced by different laser intensities were tested by ANOVA on Ranks (Kruskal-Wallis test) and Dunn's post-hoc method. The correlation between temperature at 40-μm subsurface and paw-lifting ratios was conducted by Finney Probit analysis, which is a specialized regression model of binominal response variables.[28]

3 Results

First, we measured six different laser intensities. The mean baseline temperature of 27.6 $\pm$ 1.3°C increased rapidly and reached the maximal temperature at the end of the pulse. Once the laser terminated, the temperature decreased in an exponential manner [Fig. 3(Aa)]. The longer pulse duration postponed the timing of the maximal temperature [Fig. 3(Ab)]. The spatial distributions on the skin surface were exponentially decayed from the axis of laser beam [Fig. 3(Ba)]. The peak temperature of 7 W-25 ms and 5 W-35 ms were equivalent [t-test, $p = 0.176$, Fig. 3(Bb)].

The differences of surface temperature between FEM-2 and experimental data (3.5 $\pm$ 1.7°C) was larger than that between FEM-3 and experimental data [0.8 $\pm$ 0.7°C, $p < 0.001$, Fig. 4(a)]. The heat spread was more restricted in depth in FEM-3 than in FEM-2 [Fig. 4(b)]. However, this difference was less obvious when the pulse duration was longer [Fig. 4(c)]. The correlation coefficient of surface temperature predicted by FEM-2 and FEM-3 increased from 0.992 to 0.999 when the pulse duration increased from 25 to 120 ms. Thus, we concluded that FEM-3 is more suitable to predict short-pulse laser than FEM-2.

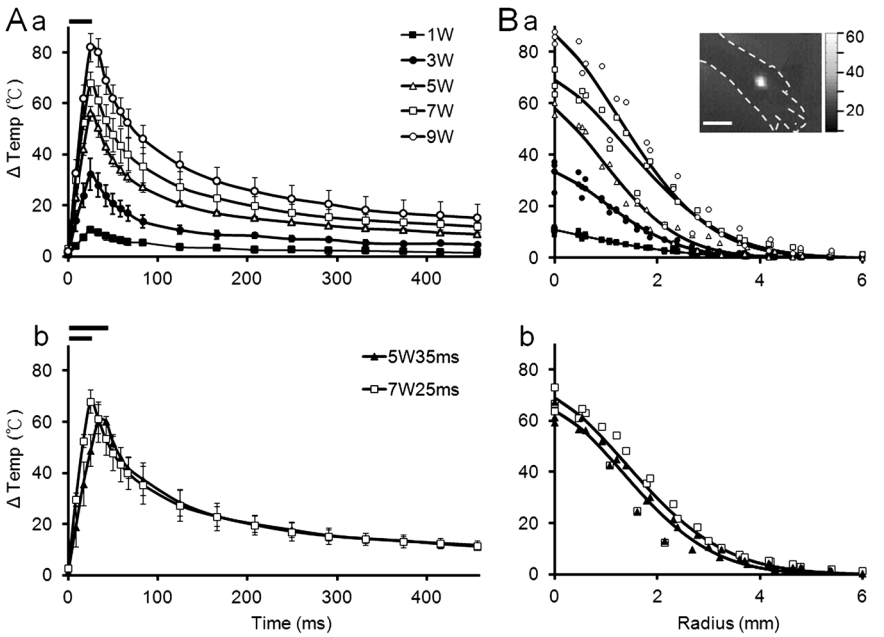

Fig. 3 Temporal and spatial temperature distribution on skin surface heated by short-pulse CO_2 laser. (A) Mean temperature distribution produced by (a) five power (1 W-, 3 W-, 5 W-, 7 W-, and 9 W-25 ms) and by (b) two pulse lengths (7 W-25 ms and 5 W-35 ms) of laser. Temperature changes were compared to baseline temperature (27.6 ± 1.3°C). The temperature rapidly reached their peaks at the end of laser pulse and exponentially decayed. Black line on top of the figure indicates laser pulse duration. Data presented by mean ± standard deviation. (B) Spatial temperature distribution was produced by five powers (a) and by two pulse lengths (b) of laser. The highest temperature was located at the center of laser and exponentially decayed along the radius. The spatial distributions are presented by exponential fitting (solid lines) from individual data (symbols). $r^2 \geq 0.94$. Inset is a 2-D isothermal map of the surface temperature of the hind paw (dotted outline) of the rat. Scale bar: 8 mm.

The surface temperature profiles predicted by FEM-3 were comparable with the experimental data [FEM-3 and Exp. Data in Fig. 5(a)]. The Pearson correlation coefficients of FEM-3 (r) were higher than 0.99. Figure 5(b) shows a peak temperature of FEM-3 and experimental data (upper panel). The peak differences of 1 W, 3 W, 5 W, 7 W, and 9 W-25 ms were 0.02°C, 1.0°C, 3.2°C, 0.5°C, and 3.5°C, respectively. The peak difference of 5 W-35 ms was 0.3°C (lower panel). Table 1 illustrates peak temperatures of measured and predicted data.

We used FEM-3 to predict subsurface temperature (Fig. 6). Because the threshold of nociceptors was assumed as 43°C[17,18] and the baseline temperature of our data was 27.6 ± 1.3°C, the baseline temperature of ≧15°C was viewed as a critical ΔT that can activate nociceptors of a rat's paw. The temperature distribution at various depths is illustrated in Fig. 6(a). The depth

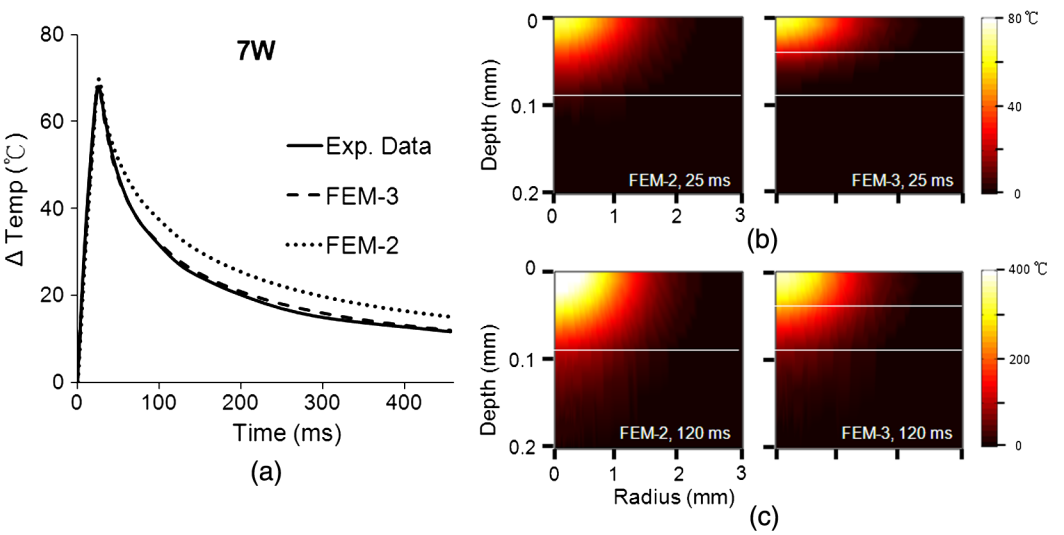

Fig. 4 Comparison of two-layer and three-layer model. (a) Temporal distribution of surface temperature changes (Δ Temp) of experimental data (Exp. Data), two-layer model (FEM-2), and three-layer model (FEM-3). The laser energy is 7 W-25 ms. (b) Temperature distribution at 25 ms of FEM-2 (left) and FEM-3 (right) of 7 W-25 ms laser. (c) Temperature distribution at 120 ms of FEM-2 (left) and FEM-3 (right) of 7 W-120 ms laser. The orientations are the same as those shown in Fig. 2.

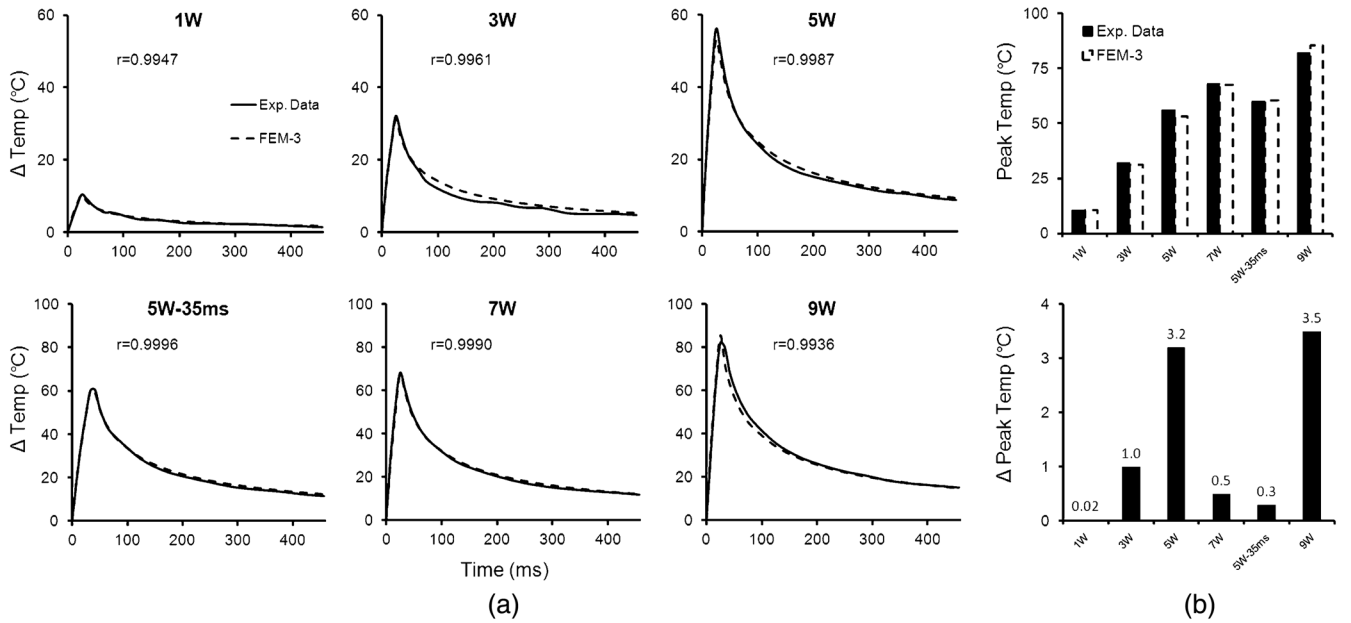

Fig. 5 Surface temperature distribution of experimental and modeling data. (a) Three-layer model (FEM-3, dash line) efficiently described experimental data (Exp. Data, solid line). *r* is the Pearson correlation coefficient of Exp. Data and FEM-3. (b) Comparison of average peak temperature (upper panel) and peak differences (lower panel) of experimental data (Exp Data) and modeling data (FEM-3) of every laser intensity.

Table 1 Temperature and paw-lifting ratio induced by short-pulse CO_2 laser. The baseline temperature was 28°C.

	Surface			Depth of 40 μm		Depth of 40 μm		Paw lifting
	Peak ΔT			Peak ΔT		Nociceptor threshold ($\Delta T \geqq 15$°C)		(%)
Laser intensity	IR (°C)	FEM-3 (°C)	Latency (ms)	FEM-3 (°C)	Latency (ms)	Onset latency (ms)	Duration (ms)	
1 W-25 ms	10.5 ± 1.2	10.5	25	4.7	41.5	—	—	0
3 W-25 ms	32.2 ± 6.2	31.1	25	14.3	41.5	—	—	29 ± 23
5 W-25 ms	56.1 ± 2.8	53.0	25	**24.9**	41.5	18.8	171.0	84 ± 20[a]
7 W-25 ms	68.0 ± 4.6	67.4	25	**32.2**	41.5	14.6	279.4	94 ± 10[a]
5 W-35 ms	60.0 ± 8.0	60.3	35	**32.3**	49.8	19.5	287.3	94 ± 6[a]
9 W-25 ms	82.0 ± 1.1	85.5	25	**39.5**	41.5	11.7	399.3	98 ± 2[a]

NOTE: Peak ΔT: peak temperature changes from the baseline temperature; IR: data measured by infrared camera (mean ± SD); FEM-3: data predicted by three-layer finite element model.
The bold numbers highlight the temperature at 40 μm subsurface that exceeded critical ΔT (15°C)
The temperature changes at 40 μm subsurface was correlated with paw-lifting ratios (Finney Probit analysis, $p < 0.001$)
[a]$p < 0.05$ compared to 1 W-25 ms and 3 W-25 ms. ANOVA on Ranks (Kruskal-Wallis test), Dunn's post hoc.

of 40 μm [dash lines in Fig. 6(a)] is the upper boundary of AMHs and CMHs (see Introduction for detail). The temperature at 40 μm of 1 W- and 3 W-25 ms (25 mJ and 75 mJ) did not reach the critical ΔT. Higher laser intensity produced longer supra-threshold duration [Fig. 6(b)] and shorter onset latency [Fig. 6(c)]. For the same laser intensity (175 mJ), the supra-threshold duration and onset latency of 7 W-25 ms (279.4 ms, 14.6 ms) was shorter than that of 5 W-35 ms (287.3 ms, 19.5 ms). Open squares in Fig. 6(b) and 6(c) indicate the data of 5 W-35 ms. Table 1 illustrates the detailed data of predicted temperature at a depth of 40 μm.

The spatial distributions of 7 W-25 ms and 5 W-25 ms are illustrated in Fig. 7(A) and 7(B). At the time point when the laser heat pulse terminated, the heat was still restricted inside the superficial layer [as in Fig. 7(A) and 7(B)]. At 1.5 and 2 times of the laser-pulse duration, the heat conducted to the surroundings and the temperature formed an isometric pattern [b and c in Fig. 7(A) and 7(B)]. The maximal radius that reached the critical ΔT at the depth of 40 μm of 5 W-, 7 W-, and 9 W-25 ms were 0.9 mm, 1.1 mm, and 1.2 mm [Fig. 7(C)], respectively.

Table 1 lists the measured, predicted peak temperature and the paw-lifting ratio of different laser intensities. On the skin surface, either measured or predicted peak temperature occurs at the end of the laser pulse. The differences of the measured

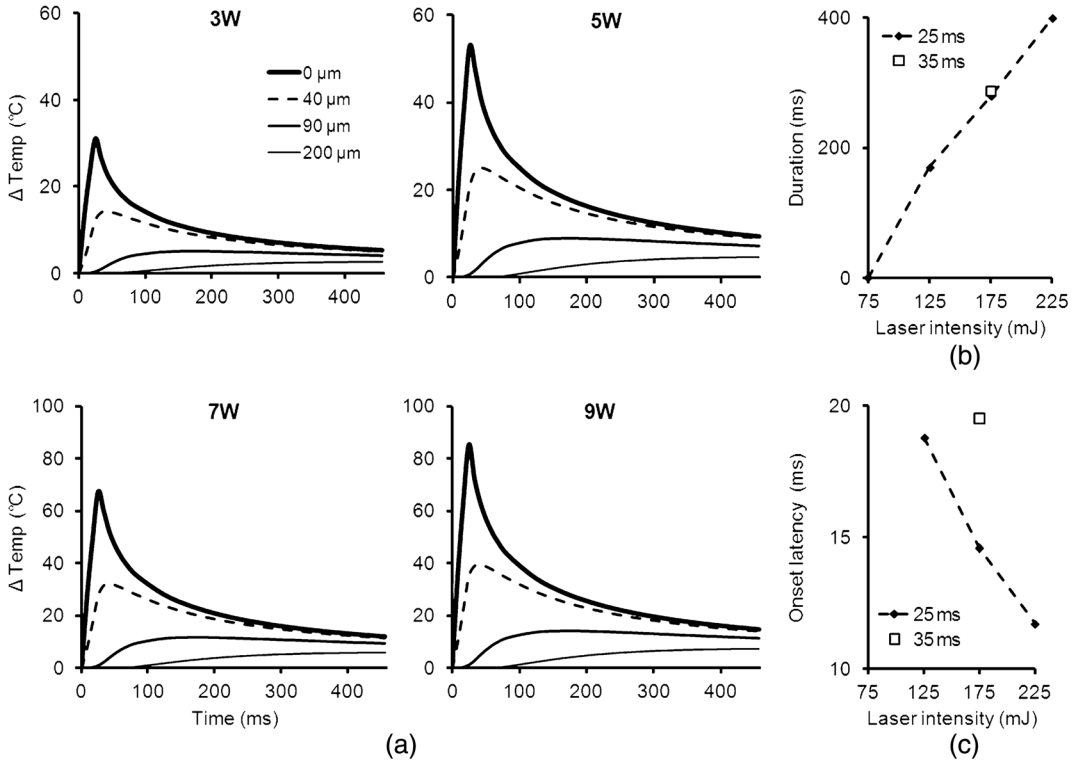

Fig. 6 Predicted temporal temperature distribution of subsurface tissue by FEM-3. (a) Temperature distribution was predicted at surface (0 μm) and three depths (40 μm, 90 μm, 200 μm) of four power. The upper and lower boundary of viable epidermis innervated by nociceptors was 40 μm (dash line) and 90 μm in depth. (b) Duration and (c) onset latency for critical temperature change ($\Delta T \geq 15$°C) at the subsurface depth of 40 μm. The open squares indicate the data of 5 W-35 ms. The laser of 75 mJ (3 W-25 ms) did not reach critical ΔT at the depth of 40 μm.

and predicted peak temperature were smaller than 3.5°C. At the 40 μm depth under the skin surface, a laser of variable intensities produced peak temperatures with a time lag comparing to the surface. Only the laser intensities higher than 5 W-25 ms produced temperature higher than critical ΔT, which may activate nociceptors. The critical ΔT occurred faster and lasted longer while the laser intensity increased. The laser intensity of 1 W-25 ms did not induce paw lifting, whereas 3 W-25 ms induced $29 \pm 23\%$ paw lifting, which did not differ from 1 W-25 ms. In contrast, the laser intensities of 5 W-25 ms, 7 W-25 ms, 5 W-35 ms, and 9 W-25 ms induced higher lifting ratio (ANOVA on Ranks with Dunn's post-hoc test, $p < 0.05$ compared to 1 W-25 ms and 3 W-25 ms). The increment of peak ΔT at depth of 40 μm correlated significantly with the

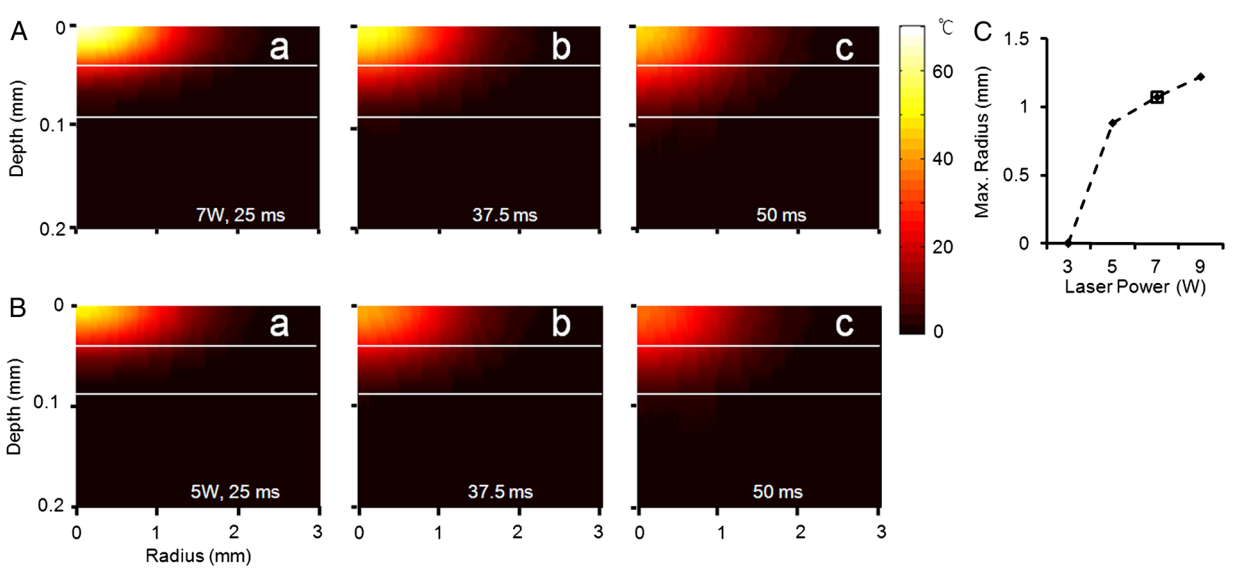

Fig. 7 Predicted spatial temperature distribution of subsurface tissue by FEM-3. Color (brightness) representations of subsurface temperature heated by (A) 7 W-25 ms and (B) 5 W-25 ms at (a) laser pulse duration, (b) 1.5 times, and (c) 2 times of laser pulse duration. (C) Maximal radius that temperature reached critical ΔT at depth of 40 μm. The open square indicates the data of 5 W-35 ms.

increment of paw-lifting ratio (Finney Probit analysis, $p < 0.001$). Hence, our prediction of nociceptors activation was validated with a nociceptive behavior index.

4 Discussion

We measured and simulated the surface temperature distribution induced by short-pulse CO_2 laser. By using three-layer finite element modeling, we predicted onset latency, supra-threshold duration, and the maximal radius that can activate nociceptors. The prediction corresponded well with the paw-lifting ratio, a commonly used nociception index of the rat.

The sampling rate of our infrared camera (120 Hz) was sufficient to detect the rapid temperature changes caused by laser heat irradiation. There were four sampling points during the 25 to 35 ms rapid heating phase and 15 sampling points during the temperature decay phase. Our prediction of short-pulse laser had smaller prediction errors than other pure predictions based on single-layer model[14,15] or two-layer model.[11] The effect of stratum corneum was less obvious when pulse duration was longer. This may be the reason that the two-layer model operated efficiently in longer pulse duration,[11] but not in this study for the short-pulse laser. We adjusted the thermal conductivity of epidermis and dermis as 0.1[24,25] and 0.2 $W/m \times K$, which was smaller than most of the human studies reported.[29–32] Because the thermal conductivity was directly proportional to water content of skin,[24] we assumed that the water content of rats' paw skin was lower than that of human skin.

Heating rate affected the threshold of escape behavior[33] and nociceptors. The paw-lifting threshold induced by 6.5°C to 7.5°C/s was approximately 52°C.[18,34] The thresholds of $A\delta$ nociceptors were 43.8 ± 0.4°C,[18] 47°C or 50°C[17] when heated at 6.5°C/s and 8°C/s. The thresholds of C nociceptors were 55.4 ± 0.7°C,[18] 37°C or 50°C[17] when heated at 6.5°C/s and 8°C/s. Our data indicated that the escape threshold was between the temperature induced by 3 W- and 5 W-25 ms, which was 42.3°C to 52.9°C.

The precise temporal profile helps to re-access the thermal effects of a CO_2 laser. The onset latency is a critical parameter when estimating conduction velocities of afferent inputs and sensory pathways. The recommendation based on our data will be to subtract the latency of activated nociceptors (onset latency) from latency of responses, especially when using lower laser power. According to the present study, the onset latency ranged from 11.7 to 19.5 ms (Table 1). The FEM-3 data indicated that the supra-threshold duration of subsurface lasts longer than laser pulse. Because the subsurface temperature remained higher than the critical temperature for 171 to 399.3 ms (Table 1), we conjecture that besides a synchronized activation of the nociceptors at the onset latency, there would be further temporal summation of additional activations in these supra-threshold temperature periods.

The diameter of receptive fields of AMH and CMH of a rat's foot are less than 1 mm in diameter.[17] A number of CMHs have larger ovoid receptive fields of 2 to 4 mm in the longer diameter.[17] Our data demonstrated that the 5 W-25 ms laser produced a heated area with maximal radius of 0.9 mm, which can activate a single nociceptor. Laser heats of 7 W- and 9 W-25 ms produced a heated area with maximal radius of 1.1 and 1.2 mm, respectively, which can activate more than one nociceptor. In this case, spatial summation of nociceptive activities may be induced.

There are many solid state infrared lasers currently in use in research and in clinics. Erbium-doped yttrium aluminum garnet (Er:YAG) emits laser of 2940 nm. The absorption coefficient of water is 10^5 m^{-1},[35] which is comparable to that of CO_2 laser. Thulium-doped YAG (Tm:YAG) emits a laser of 1930 nm. The absorption coefficient of water is 10^4 m^{-1},[36] which is less than that of a CO_2 and an Er:YAG laser. Other lasers such as neodymium-doped YAG (Nd:YAG), neodymium-doped yttrium aluminum perovskite (Nd:YAP), and diode laser emits lasers of near infrared spectrum. The absorption coefficient of water is much lower, in the range of $10^1 - 10^2$ m^{-1}[37] Argon and copper vapor laser emits lasers in visible light spectrum. The absorption coefficient of water is as low as to 10^{-2} m^{-1}.[38] Although the water absorption of lasers in near infrared and visible light spectrum is low, on the other hand, the absorption of hemoglobin and oxyhemoglobin is higher (10^5 to 10^7 m^{-1}).[39] Hence, the primary thermal effect of lasers with near infrared and visible light spectrum may be due to the absorption of hemoglobin and oxyhemoglobin, so that the results of the present study might not apply. The present results may represent Er:YAG and Tm:YAG lasers whose thermal effects are primarily caused by water absorption.

In summary, precise pain stimulator applied on animal models are critical in pain and nociception research. A short-pulse laser (tens of milliseconds) has important applications in nociception research of behavioral animals. We constructed a three-layer model that was appropriate to simulate temperature distribution of a short-pulse laser. Our results are beneficial to interpreting the physiological responses induced by CO_2 laser, as well as for assessing the thermal effects on tissue.

Acknowledgments

This research was supported by grants from the Taiwan National Science Council (NSC100-2311-B-002-002-MY3 and NSC100-2221-E-002-064) and National Health Research Institute (NHRI-EX101-10104NI).

References

1. R. Baron, "Peripheral neuropathic pain: from mechanisms to symptoms," *Clin. J. Pain.* **16**(Suppl. 2), S12–S20 (2000).
2. L. Nikolajsen and T. S. Jensen, "Phantom limb pain," *Curr. Rev. Pain.* **4**(2), 166–170 (2000).
3. J. Mor and A. Carmon, "Laser emitted radiant heat for pain research," *Pain* **1**(3), 233–237 (1975).
4. R. Kakigi, H. Shibasaki, and A. Ikeda, "Pain-related somatosensory evoked potentials following CO_2 laser stimulation in man," *Electroencephalogr. Clin. Neurophysiol.* **74**(2), 139–146 (1989).
5. B. Bromm et al., "Evoked cerebral potential correlates of C-fibre activity in man," *Neurosci. Lett.* **43**(1), 109–114 (1983).
6. R. D. Treede, J. Lorenz, and U. Baumgartner, "Clinical usefulness of laser-evoked potentials," *Neurophysiol. Clin.* **33**(6), 303–314 (2003).
7. J. L. Kramer, J. Haefeli, and C. R. Jutzeler, "An objective measure of stimulus-evoked pain," *J. Neurosci.* **32**(38), 12981–12982 (2012).
8. M. L. Tsai et al., "Differential morphine effects on short- and long-latency laser-evoked cortical responses in the rat," *Pain* **110**(3), 665–674 (2004).
9. C. C. Kuo and C. T. Yen, "Comparison of anterior cingulate and primary somatosensory neuronal responses to noxious laser-heat stimuli in conscious, behaving rats," *J. Neurophysiol.* **94**(3), 1825–1836 (2005).

10. R. J. Fan et al., "Nocifensive behaviors components evoked by brief laser pulses are mediated by C fibers," *Physiol. Behav.* **98**(1–2), 108–117 (2009).
11. K. S. Frahm et al., "Spatial temperature distribution in human hairy and glabrous skin after infrared CO_2 laser radiation," *Biomed. Eng. Online* **9**, 69 (2010).
12. M. H. Al-Saadi, V. Nadeau, and M. R. Dickinson, "A novel modelling and experimental technique to predict and measure tissue temperature during CO_2 laser stimuli for human pain studies," *Lasers Med. Sci.* **21** (2), 95–100 (2006).
13. M. J. Brugmansn et al., "Temperature response of biological materials to pulsed non-ablative CO_2 laser irradiation," *Lasers Surg. Med.* **11**(6), 587–594 (1991).
14. B. Choi, J. A. Pearce, and A. J. Welch, "Modelling infrared temperature measurements: implications for laser irradiation and cryogen cooling studies," *Phys. Med. Biol.* **45**(2), 541–557 (2000).
15. R. Haimi-Cohen, A. Cohen, and A. Carmon, "A model for the temperature distribution in skin noxiously stimulated by a brief pulse of CO_2 laser radiation," *J. Neurosci. Methods* **8**(2), 127–137 (1983).
16. S. Mense, "Anatomy of nociceptors,"Chap. 3, in *Science of Pain*, A. I. Basbaum and M. C. Bushnell, Eds., pp. 11–38, Elsevier, San Diego, CA (2009).
17. J. W. Leem, W. D. Willis, and J. M. Chung, "Cutaneous sensory receptors in the rat foot," *J. Neurophysiol.* **69**(5), 1684–1699 (1993).
18. D. C. Yeomans and H. K. Proudfit, "Nociceptive responses to high and low rates of noxious cutaneous heating are mediated by different nociceptors in the rat: electrophysiological evidence," *Pain* **68**(1), 141–150 (1996).
19. T. Ngawhirunpat et al., "Changes in electrophysiological properties of rat skin with age," *Biol. Pharm. Bull.* **25**(9), 1192–1196 (2002).
20. S. L. Kojundzic et al., "Regional differences in epidermal thickness and behavioral response following partial denervation of the rat paw," *Int. J. Neurosci.* **118**(12), 1748–1762 (2008).
21. P. Carrive, M. Churyukanov, and D. Le Bars, "A reassessment of stress-induced "analgesia" in the rat using an unbiased method," *Pain* **152**(3), 676–686 (2011).
22. R. Kakigi et al., "Pain-related magnetic fields following painful CO_2 laser stimulation in man," *Neurosci. Lett.* **192**(1), 45–48 (1995).
23. C. T. Yen, C. H. Huang, and S. E. Fu, "Surface temperature change, cortical evoked potential and pain behavior elicited by CO_2 lasers," *Chin. J. Physiol.* **37**(4), 193–199 (1994).
24. K. R. Holmes and T. Adams, "Epidermal thermal conductivity and stratum corneum hydration in cat footpad," *Am. J. Physiol.* **228**(6), 1903–1908 (1975).
25. D. Van de Sompel, T. Y. Kong, and Y. Ventikos, "Modelling of experimentally created partial-thickness human skin burns and subsequent therapeutic cooling: a new measure for cooling effectiveness," *Med. Eng. Phys.* **31**(6), 624–631 (2009).
26. H. H. Pennes, "Analysis of tissue and arterial blood temperatures in the resting human forearm," *J. Appl. Physiol.* **85**(1), 5–34 (1998).
27. R. J. de Dear et al., "Convective and radiative heat transfer coefficients for individual human body segments," *Int. J. Biometeorol.* **40**(3), 141–156 (1997).
28. D. J. Finney and W. L. Stevens, "A table for the calculation of working probits and weights in probit analysis," *Biometrika.* **35**(1–2), 191–201 (1948).
29. M. L. Cohen, "Measurement of the thermal properties of human skin. A review," *J. Invest. Dermatol.* **69**(3), 333–338 (1977).
30. S. B. Wilson and V. A. Spence, "A tissue heat transfer model for relating dynamic skin temperature changes to physiological parameters," *Phys. Med. Biol.* **33**(8), 895–912 (1988).
31. S. C. Jiang et al., "Effects of thermal properties and geometrical dimensions on skin burn injuries," *Burns* **28**(8), 713–717 (2002).
32. T. R. Gowrishankar et al., "Transport lattice models of heat transport in skin with spatially heterogeneous, temperature-dependent perfusion," *Biomed. Eng. Online* **3**, 42 (2004).
33. D. C. Yeomans and H. K. Proudfit, "Characterization of the foot withdrawal response to noxious radiant heat in the rat," *Pain* **59**(1), 85–94 (1994).
34. S. McMullan, D. A. Simpson, and B. M. Lumb, "A reliable method for the preferential activation of C- or A-fibre heat nociceptors," *J. Neurosci. Methods* **138**(1–2), 133–139 (2004).
35. J. T. Walsh, Jr. and T. F. Deutsch, "Er:YAG laser ablation of tissue: measurement of ablation rates," *Lasers Surg. Med.* **9**(4), 327–337 (1989).
36. E. D. Jansen et al., "Temperature dependence of the absorption coefficient of water for midinfrared laser radiation," *Lasers Surg. Med.* **14**(3), 258–268 (1994).
37. J. A. Curcio and C. C. Petty, "The near infrared absorption spectrum of liquid water," *J. Opt. Soc. Am.* **41**(5), 302–304 (1951).
38. R. M. Pope and E. S. Fry, "Absorption spectrum (380–700 nm) of pure water. 2. Integrating cavity measurements," *Appl. Opt.* **36**(33), 8710–8723 (1997).
39. B. L. Horecker, "The absorption spectra of hemoglobin and its derivatives in the visible and near infra-red regions," *J. Biol. Chem.* **148**(1), 173–183 (1943).